RESEARCH ARTICLE

Macromolecular Rapid Communications
www.mrc-journal.de

4D Fabrication of Two-Way Shape Memory Polymeric Composites by Electrospinning and Melt Electrowriting

*Chiara Pasini, Zhander Vohr Soreño, Dennis Schönfeld, Thorsten Pretsch, Gissela Constante, Ilia Sadilov, and Leonid Ionov**

This work presents a new method for 4D fabrication of two-way shape memory materials that are capable of reversible shapeshifting right after manufacturing, upon application of proper heating and cooling cycles. The innovative solution presented here consists in the combination of highly stretched electrospun shape memory polymer (SMP) nanofibers with a melt electrowritten elastomer. More specifically, the stretched nanofibers are made of a biocompatible thermoplastic polyurethane (TPU) with crystallizable soft segments, undergoing melt-induced contraction and crystallization-induced elongation upon heating and cooling, respectively. Reversible actuation during crystallization becomes possible due to the elastic recovery of the elastomer component, obtained by melt electrowriting of a commercial TPU filament. Thanks to the design freedom offered by additive manufacturing, the elastomer structure also has the role of guiding the shape transformation. Electrospinning and melt electrowriting process parameters are set up so to obtain smart 4D objects capable of two-way shape memory effect (SME), and the possibility of reversible and repeatable actuation is demonstrated. The two components are then combined in different proportions with the aim of tailoring the two-way SME, taking into account the effect of design parameters such as the SMP content, the elastomer pattern, and the composite thickness.

1. Introduction

Among the various types of shape-changing polymers, bidirectional actuating shape-memory polymers (SMPs) show significant potential. They possess the unique ability to reversibly actuate themselves, typically by simply applying proper thermal cycles,[1] as opposed to SMPs exhibiting the so-called "one-way shape memory effect," which require manual deformation for every thermoresponsive shape change.[2] Moreover, bidirectional actuating SMPs can work in a wide range of environments, which sets them apart from hydrogels,[3] and they are obtained through relatively straightforward synthesis, unlike the more complex process involved in creating liquid crystalline elastomers (LCEs).[1]

The two-way shape memory effect (SME) exhibited by these materials relies on altering the conformation of the polymer chains and generating or releasing stress during the processes of melting and crystallization.[4] Considering single material systems with bidirectional actuation capability, crystallizable polymer network structures turn out as a useful starting point. For instance, in polymers with a phase segregated structure such as thermoplastic polyurethanes (TPUs), the network consists of hard segments and soft segments, of which the latter exhibit a crystallization/melting transition. It is this phase transition behavior, which can be considered as a basis for the two-way SME when bringing polymers in a state of higher order through elongation. As soon as stress- and/or cooling-induced soft segment crystals undergo melting, internal stresses are released and the polymer chains shift into a coiled conformation, causing the polymer to contract or build up stress, depending on whether it is kept in a stress-free state or under tension. In turn, cooling-induced recrystallization of the soft segments along the direction of the previously applied elongation leads to the extension of the polymer. In this way, changes in length can be thermoreversibly activated.[5]

There are plenty of examples of SMPs exhibiting a two-way SME, proposed above all as soft actuators and for applications in the biomedical field, such as bandages, temporary fixation parts, active devices to help disabled people, shape-switching drug carriers, and dynamic mechanical stimulation of cell cultures.[6–8] Particular attention has been dedicated to SMP fibrous structures

C. Pasini
Department of Mechanical and Industrial Engineering
University of Brescia
via Branze 38, Brescia 25123, Italy

Z. V. Soreño, G. Constante, I. Sadilov, L. Ionov
Faculty of Engineering Sciences
University of Bayreuth
Ludwig Thoma Str. 36A, 95447 Bayreuth, Germany
E-mail: leonid.ionov@uni-bayreuth.de

D. Schönfeld, T. Pretsch
Shape Memory Polymers Group
Fraunhofer Institute for Applied Polymer Research IAP
Geiselbergstr. 69, 14476 Potsdam, Germany

L. Ionov
Bavarian Polymer Institute
University of Bayreuth
95447 Bayreuth, Germany

The ORCID identification number(s) for the author(s) of this article can be found under https://doi.org/10.1002/marc.202400010

DOI: 10.1002/marc.202400010

obtained by electrospinning, exhibiting faster shape recovery than the bulk material because of higher mobility and larger specific surface area for heat exchange.[9,10] A variety of applications of electrospun SMPs is listed in literature, especially addressing tissue engineering, drug delivery, and electronics,[11,12] and recently, also exploiting materials with bidirectional actuation (e.g., polyurethane membranes with temperature tunable pores under constant stress;[13] electrospun LCE micro-actuators;[14] and poly(ϵ-caprolactone) smart scaffolds[15]).

The fabrication process of these materials must include a deformation step to stretch the semicrystalline network and enable bidirectional actuation between two states, one closer to the stretched shape and the other closer to the permanent one. A particularly simple preparation route is that of attaching an elastomer to a deformed SMP; SMP–elastomer composites exhibit stress-free two-way SME, thanks to the internal stresses that are generated/released during melting/crystallization of the pre-stretched SMP, but they still require a dedicated processing step for SMP deformation.[16–18] Fabrication of already stretched structures capable of unidirectional or bidirectional actuation is reported seldom: for example, by electrospinning on a rotating drum,[19] or by 3D printing polymers in viscoelastic state under properly selected printing conditions.[20,21]

This paper presents a new method for 4D fabrication of bidirectional shape memory polymeric composites that are ready to actuate, right after manufacturing using a combination of fiber spinning techniques. First, a TPU with crystallizable soft segments, which has already shown good shape memory capabilities as well as excellent biocompatibility,[22–24] is processed by solution electrospinning (SES), enabling the deposition of fibers in a stretched state. Then, an elastomeric structure is printed onto the electrospun nanofibers by melt electrowriting (MEW), a technology that allows creating compliant structures with improved resolution and controlled complex morphologies, bridging the gap between SES and direct-write 3D printing processes.[25–28] The stretched SMP fibers tend to shrink at temperatures above the melting point of the soft segments, whereas MEW fibers are deposited in a stress-free state and resist the shrinking, guiding the overall shape transformation over time (i.e., the 4th dimension). The reversibility of the shape changes is obtained by cooling below the crystallization temperature of the SMP soft segments.

Their two-way actuation distinguishes the resulting smart structures from other 4D-printed objects realized by printing polymers on pre-stretched textiles/sheets[29,30] or by inkjet printing SMP–elastomer laminates;[31] in particular, the presence of a SMP and the integration of high pre-stretch/molecular orientation must be both provided for bidirectional actuation. An alternative path is 4D-printed LCEs that can reversibly shapeshift by combining the anisotropic properties of mesogens and the entropy elasticity of lightly cross-linked polymer networks;[32] however, printing these materials can be complex and expensive, and current mesogen alignment strategies are still rather limited.[33] Conversely, the process developed in this work is much easier to perform, and it offers the possibility of tailoring the two-way SME by acting on design parameters such as the SMP/elastomer proportions, the SMP pre-stretching, the elastomer pattern, and the bilayer thickness. Moreover, an additional advantage of the obtained materials is their flexibility, provided by their fibrous structure.

2. Results and Discussion

2.1. Working Principle and Fabrication of the Shape Memory Composites

The two-way shape memory effect (SME) of the materials described in this paper relies on the combination of a pre-stretched shape memory polymer (SMP) with an elastomer, which is among the strategies proposed by the literature to achieve such effect.[1] Compared to more conventional casting/molding methods previously described,[16–18] a new fabrication process is here proposed which i) integrates pre-stretching directly in the SMP manufacturing phase by solution electrospinning (SES) and ii) guarantees higher flexibility in the design of shape changes thanks to additive manufacturing of the elastomer component by melt electrowriting (MEW). More in detail, the steps concerning the realization and thermal activation of these smart materials are represented in **Figure 1**.

First, a shape memory thermoplastic polyurethane (TPU) with 75% poly(1,4-butylene adipate) (PBA)-based soft segments (TPU PBA-75) is synthesized and employed in the production of the active layer due to the good shape memory properties observed in a recent study.[22] Its thermoresponsive behavior is given by its physically cross-linked molecular structure, containing 75% PBA-based crystallizable soft segments. In fact, the polymer can be deformed into a temporary shape above PBA melting temperature (T_m) and cooled down below PBA crystallization temperature to crystallize the soft segments and fix the deformation; in a second moment, it can be heated up above T_m to melt the PBA crystals and recover the original shape stored in the hard segments. Another study[24] also highlighted important advantages of TPU PBA-75 for applications in soft tissue engineering, including biocompatibility, biodegradability and low elastic modulus in the range of a few MPa. TPU PBA-75 is dissolved in organic solvents to be processed by SES (Figure 1a). The electrospinning parameters, solution composition, and collector type are adjusted as described in Section 2.1.1., aiming at obtaining a mat of highly stretched nanofibers on the support substrate.

In a second stage (Figure 1b), an elastomer is deposited onto the electrospun mat as passive component, intended to guide the overall shape transformation and ensure its reversibility. To these ends, MEW technique is adopted for higher control over the geometry of the system, and a commercial elastomer (TPU Filaflex 70A) is selected for being stable above PBA T_m and good at storing and recovering deformations in the elastic field. In addition, this second material has low elastic modulus (≈7 MPa[34]), guaranteeing sufficient shape change upon actuation. The MEW pattern, thickness, and process parameters are tailored as reported in Section 2.1.2. The obtained samples, still attached to the support substrate, are then stored in a freezer (Figure 1c) to fix the electrospun nanofibers in their stretched configuration by crystallization of TPU PBA-75 soft segments.

The tensile deformation in the nanofibers is partially lost when the samples are detached from the support substrate at room temperature (T_{room})—the nanofiber side contracts, that results in bending of the bilayer (Figure 1d)—and further released by melting PBA-based crystals at a temperature $T_{high} > T_m$ (Figure 1e). The presence of the elastomer hinders the contraction of the SMP, resulting in bending of the specimens toward the SMP

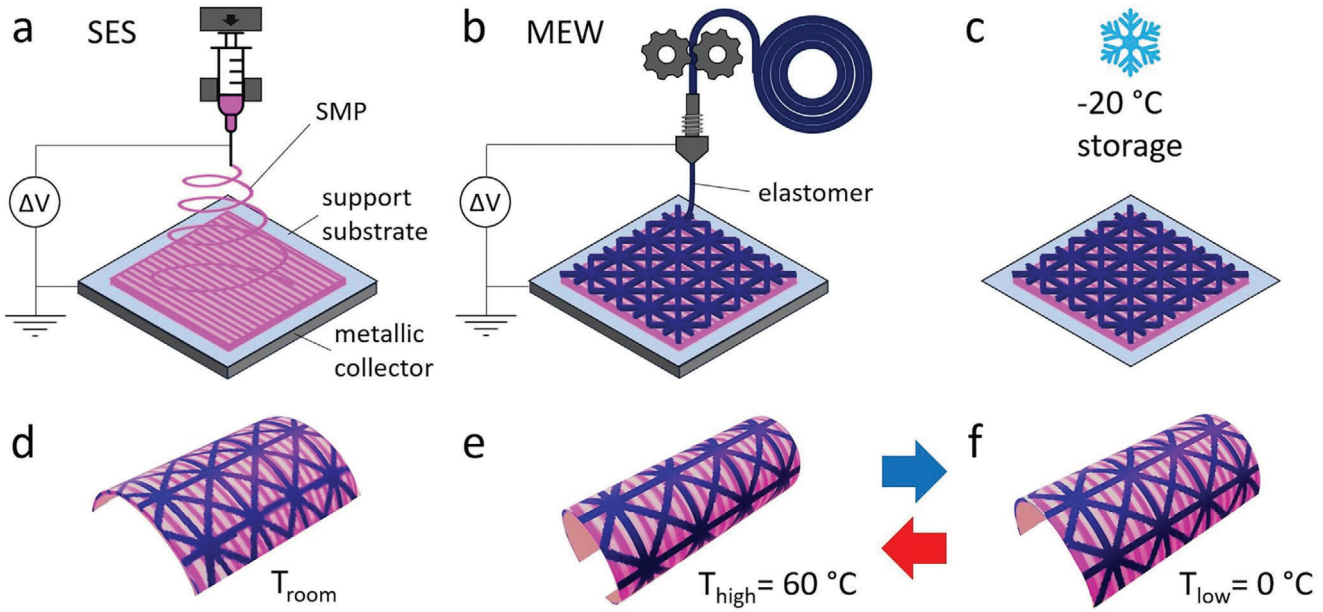

Figure 1. Steps for 4D fabrication of the two-way shape memory composites: a) SES of the SMP on a support; b) MEW of the elastomer onto the SMP; c) cooling and storage in freezer; d) shrinking upon support removal at T_{room}; e) closed configuration upon heating up to T_{high}; f) open configuration upon cooling down to T_{low}. The transformation between (e) and (f) is reversible and repeatable.

side. By cooling the composite material down to a temperature T_{low}, below PBA segments crystallization temperature, the deformed elastomer is expected to provide sufficient stress for crystallization-induced elongation in the SMP, reducing bending of the specimens (Figure 1f), similar to what has been previously observed when an external stress is applied to TPU PBA-75 during heating–cooling cycles.[23] Further applications of T_{high} and T_{low} should lead again to the more closed configuration in Figure 1e and the more open configuration in Figure 1f, respectively; therefore, reversible and repeatable two-way SME is achieved.

Aiming to choose suitable values of T_{high} and T_{low}, DSC analysis was carried out on TPU PBA-75, with particular focus on observing the crystallization during isothermal stages at different T_{low} values (10 °C; 0 °C; −10 °C; −20 °C). For each temperature considered, a complete heating–cooling cycle was performed, that is, heating up to 80 °C, waiting for 5 min, cooling down to T_{low}, and maintaining for 4 h. The thermograms of all DSC heating scans are displayed in **Figure 2a**, while Figure 2b plots the specific heat flow against time during the cooling steps and the isothermal steps at T_{low}; the origin of the time axis is set at the beginning of the isothermal tracts.

The heating scans present a main endothermal peak at ≈40–45 °C, which is associated with the melting transition of the soft segments. When heating follows one of the 4 h isotherms at T_{low}, the melting process begins earlier and the peak temperature tends to be reduced with respect to the first heating scan; such differences can be explained considering that PBA crystallized segments in the original granules have much more time to rearrange and stabilize their molecular structure at T_{room} ($<T_m$) with respect to those formed during 4 h at T_{low}. However, in all the cases, the melting process is finalized within 50–55 °C; therefore, T_{high} can be reasonably set to 60 °C during the shape memory experiments. Moreover, a degree of crystallinity of ≈17% can be estimated by comparing the melting enthalpy of 100% crystalline PBA (135 J

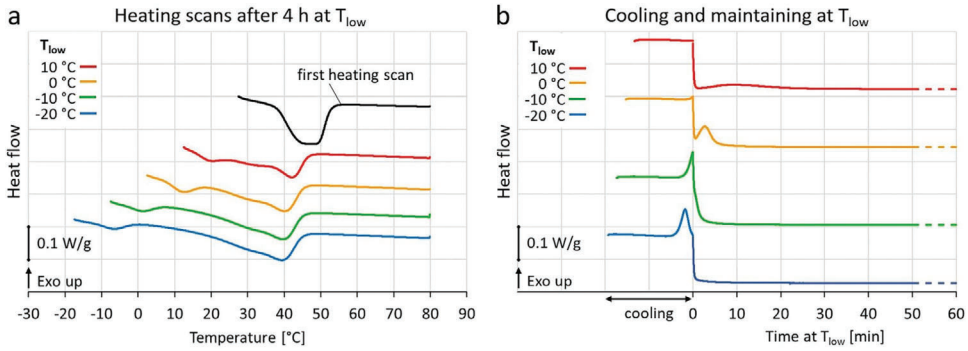

Figure 2. Results of DSC analyses: a) heating scans as a function of temperature; b) cooling and isothermal steps as a function of time.

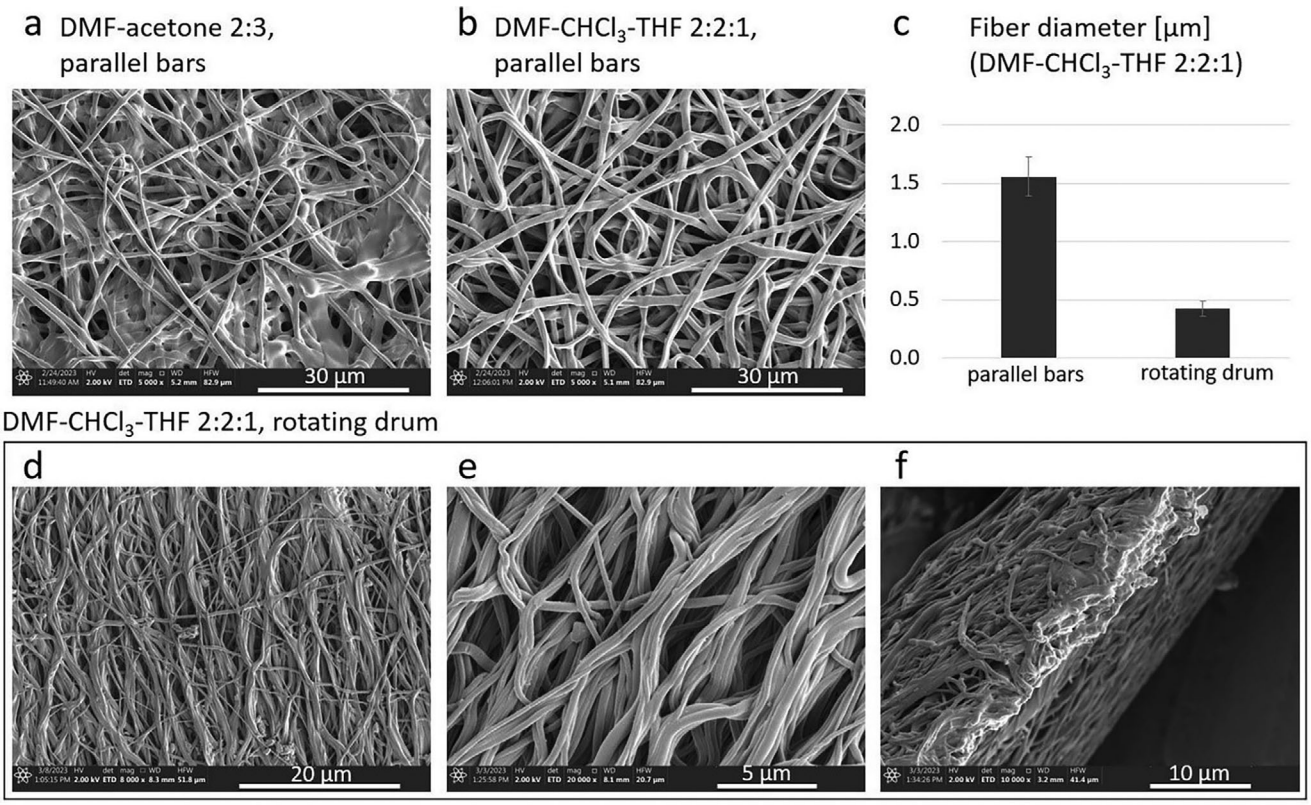

Figure 3. a,b,d–f) SEM images of electrospun fibers obtained by using different solvents and collectors and c) diameter values for fibers obtained with the best solvent on different collectors.

g^{-1})[35] with that in the thermograms (16–18 J g^{-1}, where applicable, i.e., when a sufficiently reliable baseline could be defined).

The effect of the selected T_{low} on the crystallization of SMP soft segments can be appreciated by looking at the associated exothermal signals in Figure 2b. At 10 °C, a long time is required for crystallization, which mostly occurs in less than 10 min at 0 °C and even before the beginning of the isothermal stage for the lowest values of T_{low}. In fact, the nucleation of crystals is faster at lower temperatures. At the light of these findings, the specimens are stored in a freezer at −20 °C to promptly fix the electrospun nanofibers in their stretched configuration, whereas the shape memory experiments are performed with T_{low} = 0 °C, which is more convenient to handle and still allows short cooling times. However, it should be specified that, while crystal nucleation slows down when approaching T_m, crystal growth becomes faster, still allowing to obtain high crystallinity in the long time.

2.1.1. SES Setup

A good pre-stretching of the SMP is fundamental for the achievement of the two-way SME without applying any external stress to the SMP–elastomer composites. Therefore, the effects of several variables were considered until obtaining nanofibers with the desired morphology and shrinking upon heating.

First, different values of flow rate (0.25–0.5–1 mL h^{-1}), applied voltage (20–25–30 kV), and solution concentration (6–8–10 w/v%) were compared. A dimethylformamide-acetone (DMF–acetone) mixture with volume ratio of 2:3 was employed as solvent, based on the previous use of these two chemicals in touch-spinning of a TPU PBA-75 solution.[24] All conditions allowed SES except for the highest TPU concentration (10%), which appeared to excessively increase the solution viscosity. The nanofibers were collected on glass slides on two parallel conductive bars and observed at the optical microscope (images in Figure S1a, Supporting Information). Looking for thin nanofibers with a regular morphology, the voltage was set at 25 kV, the flow rate at 1 mL h^{-1}, and the concentration at 6 w/v%. In particular, the fiber diameter (Figure S1b, Supporting Information) did not significantly vary with the voltage and flow rate; conversely, reducing the solution concentration to 6 w/v% was more effective; though, the final fibers had still quite large diameter (2 µm).

For fibers obtained with the selected process parameters, a further morphology check by means of scanning electron microscope (SEM) and some shrinking tests were carried out. SEM images revealed several areas in which the fibers appeared fused together due to incomplete evaporation of the solvent (**Figure** 3a), which led to substitute DMF-acetone (2:3) with a new mixture of solvents. Figure 3b reports the improvement achieved by using dimethylformamide-chloroform-tetrahydrofuran (DMF-$CHCl_3$-THF) with volume ratios of 2:2:1, which was employed in the production of all specimens from here on. Moreover, the shrinkage of electrospun mats at 60 °C was barely noticeable (Figure S2a, Supporting Information). It was concluded that the application of high voltage was insufficient to effectively stretch TPU PBA-75, probably because of its

high molecular weight (≈1.4×10^5 g mol^{-1}).[24] For this reason, the electrospinning setup was finalized by using a rotating drum as collector and selecting a high rotation speed (8000 rpm), aiming at mechanically drawing the fibers. The values of fiber diameter obtained before and after this improvement are illustrated in Figure 3c, and SEM images of the new materials are provided in Figure 3d–f. While fibers collected on parallel bars are randomly oriented and rather thick (diameter of ≈1.6 µm), the new samples consist of thinner nanofibers (diameter of ≈0.4 µm) mainly aligned along the circumferential direction of the rotating drum; an overall thickness of a few microns is achieved in 1 h of SES.

The reduced diameter of the nanofibers is indicative of their stretched state, which is confirmed by the significative shrinking of the electrospun mats after freezing (to fix the deformation at best) and detaching from the collector. Due to the preferential alignment of the nanofibers, most of the shrinkage occurs along the circumferential direction of the drum (≈15%) while the axial contraction is limited (≈5%). At T_{high} = 60 °C, the crystalline domains responsible for shape fixation melt, and the specimens further contract until reaching shrinking values of ≈50% in the circumferential direction and 10% in the axial direction (Figure S2b, Supporting Information). This experiment highlights that while both parallel bars and rotating drum allow production of nanofibers, the fibers produced by the two methods are different: fibers produced using a rotating drum are strongly oriented and stretched while those produced using parallel bars are not. By comparing fiber diameter values obtained with the two collector types and considering the volume of fibers as constant, it is also possible to approximately quantify the fiber stretching achieved by means of the drum rotation: $(l_2 - l_1)/l_1 = l_2/l_1 - 1 = (d_1/d_2)^2 - 1 \approx 1280\%$, where l_1 and d_1 are the length and the diameter of fibers collected on parallel bars while l_2 and d_2 are those of fibers collected on the rotating drum.

2.1.2. MEW Setup

The next step was the selection of MEW parameters for TPU Filaflex. The effects of nozzle temperature and applied voltage were first explored, maintaining the collector speed at its maximum value (1800 mm min^{-1}) and a distance of 3 mm between nozzle and collector. Figure S3a, Supporting Information shows diameter values and optical microscope images of the obtained fibers, as well as viscosity versus shear rate curves and viscosity versus shear stress curves at 230 °C and 240 °C. The highest voltage applied (3.5 kV) excessively accelerates the molten polymer flow, so that the collector is not fast enough to collect straight fibers, and wavy thin fibers are produced. Better results are obtained by reducing the voltage, leading to less stretched fibers having larger diameter. More in detail, for a nozzle temperature of 230 °C, a voltage decrease from 3.5 to 1.5 kV increases the diameter from ≈50 µm to ≈110 µm. For a temperature of 240 °C, the lower viscosity of the melt seems to ease the flow of a larger amount of material through the nozzle (corresponding to thicker fibers, e.g. 80 µm diameter with a voltage of 3.5 kV) and to produce more irregular fibers (especially under application of 1.5 kV, resulting in counter-trend thin filaments interrupted by long bead defects[36]). Moreover, rheological curves at 240 °C are more irregular: deviations at low stress seem to indicate a thixotropic behavior, probably occurring when hydrogen bonds between polymer chains break and the polymer melt starts flowing; deviations at high stress may be ascribed to transition to elastic regime and failure. In the end, a nozzle temperature of 230 °C and an applied voltage of 2.5 kV are selected as the most reliable set of parameters. The final fiber diameter is ≈80 µm, slightly increasing up to ≈90 µm when printing on top of electrospun mats; this is because covering part of the conductive collector with the SMP mitigates the voltage effect to some degree.

In addition, it was observed that MEW was not accurate when changing the travelling direction of the extruder due to jet lagging. This problem was solved by reducing the collector speed in correspondence of turns in the deposition path. For all values of collector speed adopted, the corresponding shear rate values in the MEW device nozzle (≈$4 \div 26$ s^{-1}) were in the stable range of rheological curves (Figure S3a, Supporting Information); although during MEW (between nozzle and collector) the polymer experiences elongational deformation rather than shear, these measurements can be associated with the fact that the molten polymer flowed in Newtonian flow regime and was deposited in a relaxed state on the collector. As reported in Figure S3b, Supporting Information, the highest accuracy was achieved by setting the collector speed to 600 mm min^{-1} since 2 mm before changing travelling direction, until the turn was completed. It was also noticed that, regardless of the selected speed, the deceleration of the extruder in proximity of turning points inevitably caused some accumulation of material and a consequent local increase in fiber diameter (up to 120–150 µm).

2.1.3. Fabrication of SMP–Elastomer Composites

The composite nature of the shape memory materials proposed in this study provides versatility to the adopted 4D fabrication strategy. In fact, the shape transformation can be modulated by acting on the stiffness of each component. In particular, the electrospun mat stiffness depends on its thickness (which is directly proportional to the associated nominal mass of 4 cm^2 samples) while that of the MEW part can be locally tailored by designing and printing specific patterns, as well as by changing the number of printed layers. Both the thickness ratio of the active and passive components and the total thickness of the specimen are expected to affect the final result.

Table 1 summarizes all the SMP–elastomer combinations that are explored, labeling them according to their SMP/elastomer thickness ratio. The SMP layer has three possible values of associated nominal mass (0.5–1–2 mg), corresponding to different values of surface density. Moreover, the MEW part has four possible values of surface density, depending both on the number of printed quasi-isotropic sequences ($N = 1$ or $N = 2$) and on the density of single layers (the standard corresponds to 1 mm fiber spacing, while higher density areas have 0.5 mm fiber spacing and are indicated with a "d" in the label in Table 1).

The appearance of quasi-isotropic MEW structures is displayed in **Figure 4a** for standard density and $N = 1$ or $N = 2$. In addition, Figure 4b reports SEM images of a 0.5/1 composite, providing a first rough estimation of the SMP/elastomer proportions based on thickness measurements, that is, (3.7 ± 0.9) µm for 0.5 mg electrospun mats and (360 ± 70) µm for MEW

Table 1. Summary of all explored SMP–elastomer combinations.

Label	SES		MEW		Estimated thickness ratio
	Nominal mass (4 cm^2) [mg]	Surface density [mg cm^{-2}]	Number of sequences ($[0°/45°/90°/-45°]_s$) [%]	Surface density [mg cm^{-2}]	
2/2	2	0.49 ± 0.03	2	15.6 ± 1.1	1/50
2/2d	2	0.49 ± 0.03	2 (with higher density)	31.2 ± 2.2	—
1/2	1	0.26 ± 0.03	2	15.6 ± 1.1	1/100
1/2d	1	0.26 ± 0.03	2 (with higher density)	31.2 ± 2.2	—
0.5/2	0.5	0.13 ± 0.02	2	15.6 ± 1.1	1/200
0.5/1	0.5	0.13 ± 0.02	1	7.8 ± 0.6	1/100

structures with $N = 1$. As detailed in Table 1, the thickness ratio of 0.5/1 and 1/2 composites is ≈1/100, that of 0.5/2 composites is ≈1/200, and that of 2/2 composites is ≈1/50. SMP mass fraction values are also calculated on the basis of the surface density of the two components and illustrated in Figure 4c for all the considered alternatives. Small TPU PBA-75 contents are obtained, overall ranging between 0.7% and 3%.

Two specimen shapes are created for shape memory experiments: i) a C shape is simply achieved for specimens having uniform thickness and thickness ratio (**Figure 5a**) and ii) a S shape is the result of a more complex MEW pattern, combining two standard density areas printed on different sides of the electrospun mat (the two curves of the S) and three higher density areas (extremities and center of the S), as shown in Figure 5b.

2.2. Two-Way SME Characterization

The shape memory behavior of SMP–elastomer composites and its tunability were investigated by applying proper heating–cooling cycles in water; this minimized possible gravity and friction effects. C-shaped samples were employed to study the possibility of achieving a stress-free two-way SME, as well as the impact of specimen thickness and SMP content. More specifically, C-shaped specimens were prepared with SMP/elastomer thickness ratios equal to 2/2, 1/2, 0.5/2, and 0.5/1.

Figure 6a shows that all specimens partially bend at T_{room} upon removal of their stiff substrate and further bend upon heating up to 60 °C; the resulting values of curvature (κ) are reported in Figure 6b. The observed curvature depends on the balance between the force generated by contracting electrospun fibers and the mechanical resistance of the passive layers. Therefore, remarkable shapeshifting occurs when heating above TPU PBA-75 transition temperature due to the release of the tensile deformation stored in PBA-based crystalline domains.

The most evident effect is that of the total thickness of the specimens. In fact, considering a same thickness ratio of 1/100 (i.e., 0.5/1 and 1/2 composites), thinner constructs exhibit remarkably

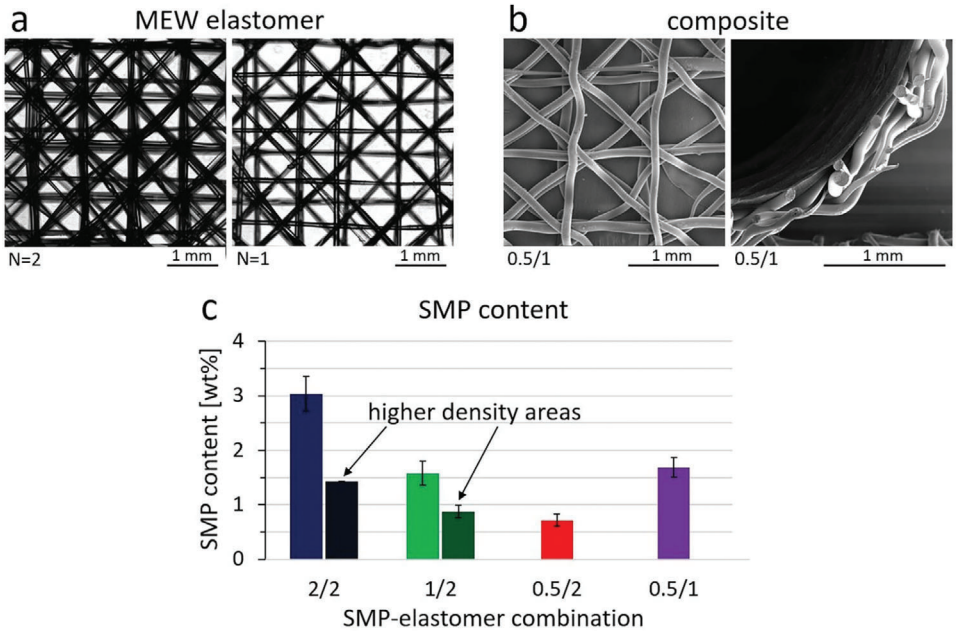

Figure 4. a) N quasi-isotropic sequences printed by MEW and observed at the optical microscope. b) Example of shape memory composite observed at SEM from the top and side views. c) Mass fraction of SMP for all SMP-elastomer combinations in Table 1.

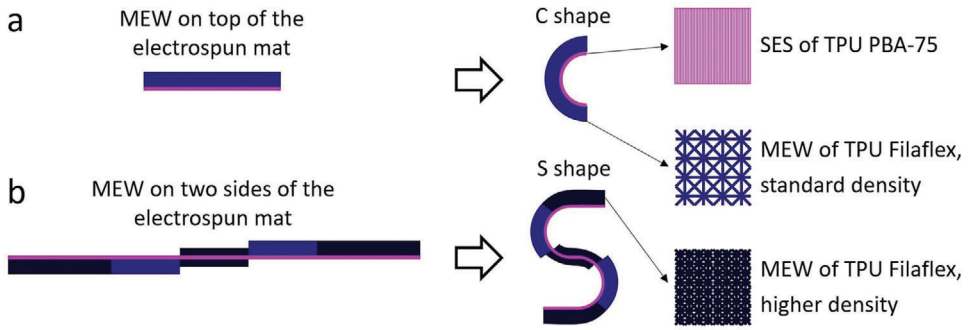

Figure 5. Schematic representation of specimens designed to take on a) a C shape or b) an S shape, with indication of fabrication techniques and materials employed for areas highlighted in different colors.

higher κ values (380 m^{-1} vs 85 m^{-1} at T_{room}; 1200 m^{-1} vs 450 m^{-1} at T_{high}). The excessive coiling of 0.5/1 composites at T_{high} does not favor the two-way SME, which may be hindered by friction between contact surfaces.

Conversely, the effect of the SMP content appears modest when comparing specimens consisting of the same MEW structure (2 quasi-isotropic sequences) but different electrospun layer thickness, namely 2/2, 1/2, and 0.5/2 composites. At T_{room}, overall similar curvatures are measured, but some 0.5/2 specimens bend more than the others due to partial delamination starting at their edges; delamination at the interface between the double MEW structure and the thinnest electrospun mat becomes complete upon heating, leading to discarding this combination. It is hypothesized that, when heating a composite with the highest thickness ratio between the elastomer and the SMP components, the contraction force due to the thin electrospun mat overcomes inter-layer adhesive forces more easily than winning against the mechanical resistance of the thick MEW structure. At T_{high}, higher SMP content corresponds to slightly increased κ values (520 m^{-1} for 2/2 composites vs 450 m^{-1} for 1/2 composites); even if these values are rather close from a statistical point of view, this trend appears reasonable because the contraction of SMP pre-stretched fibers is indeed the driving force for the composite bending.

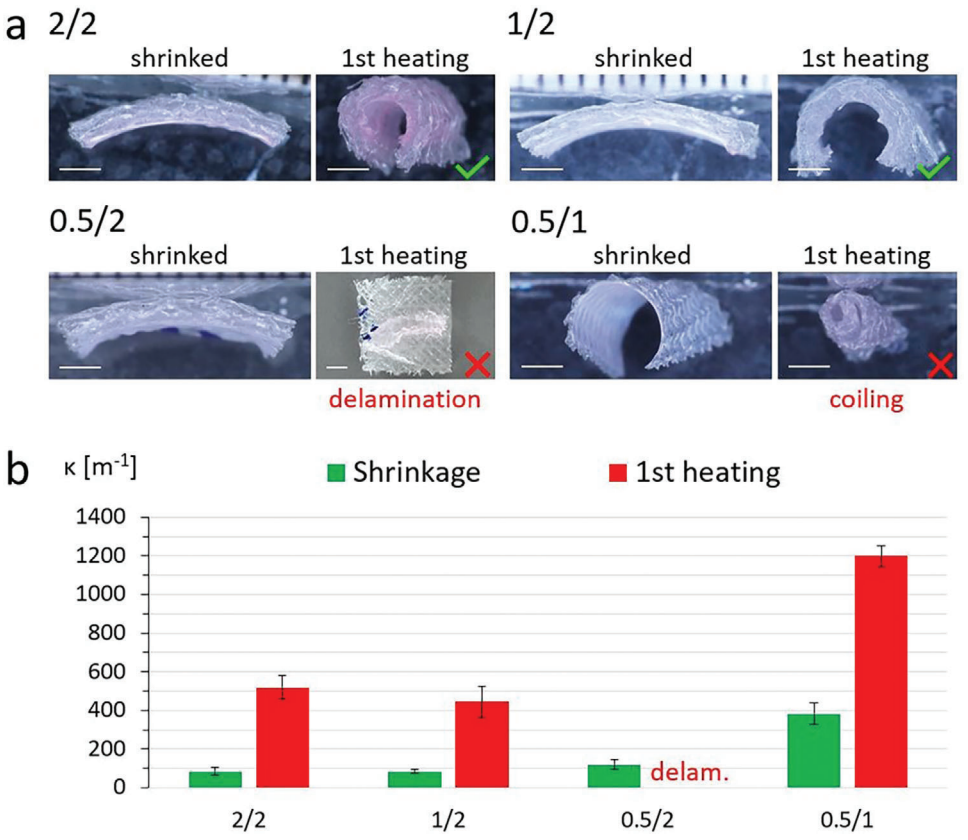

Figure 6. a) Images and b) curvature measurements of various SMP–elastomer combinations after shrinking at T_{room} and after first heating at 60 °C.

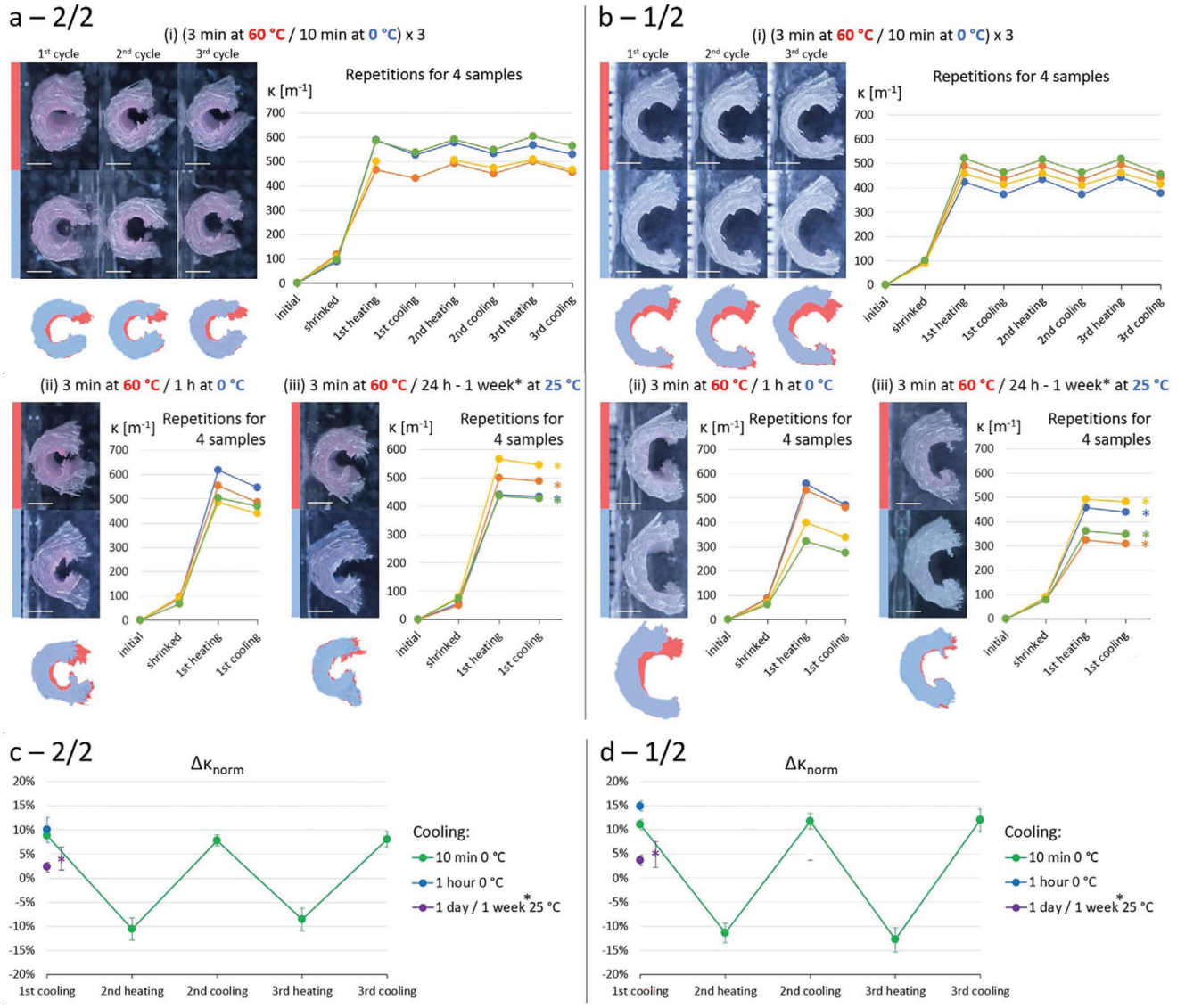

Figure 7. Two-way SME of 2/2 and 1/2 C-shaped specimens during various heating–cooling cycles: a,b) images, visual comparison, and curvature measurements; c,d) curvature variations, normalized with respect to the effect of first heating.

These data allow drawing two guidelines for further investigations: i) among the SMP–elastomer combinations considered, only 2/2 and 1/2 appear promising in view of SME reversibility and ii) the total thickness of the systems plays a major role in their shape transformations and it does not significantly change with the SMP content because the microscopic thickness of the electrospun mats can be reasonably neglected.

Once the desired C shape is guaranteed upon heating, the two-way SME can be assessed. While heating triggers the contraction of the electrospun SMP, cooling under an external tensile stress induces recrystallization of its soft segments in a stretched configuration. Here, the stress is provided by the elastic recovery of the elastomer, which is expected to decrease the C curvature. The results of this approach are documented in **Figure 7**, reporting the effect of various heating–cooling cycles on 2/2 and 1/2 composites.

More in detail, images and κ values of 2/2 and 1/2 specimens are illustrated in Figures 7a and 7b, respectively, for three thermal histories: i) 3 min at 60 °C followed by 10 min at 0 °C, repeated for three successive cycles; ii) 3 min at 60 °C followed by 1 h at 0 °C; iii) 3 min at 60 °C followed by 1 week at ≈25 °C (collecting data after 1 day and 1 week at T_{room}). Both types of specimens exhibit reversible SME, closing at T_{high} and opening at T_{low}, and the feasibility of multiple actuations is also demonstrated in both cases. More precisely, the effect is clearly visible when the cooling temperature is equal to 0 °C, after 10 min as well as after 1 h, whereas the opening of samples maintained at T_{room} is barely perceptible. This is consistent with DSC data, showing that a temperature of 10 °C or higher is not optimal for efficient crystallization of TPU PBA-75.

In addition, Figure 7c,d better highlights the amount of deformation that is reversibly gained and released at each cooling

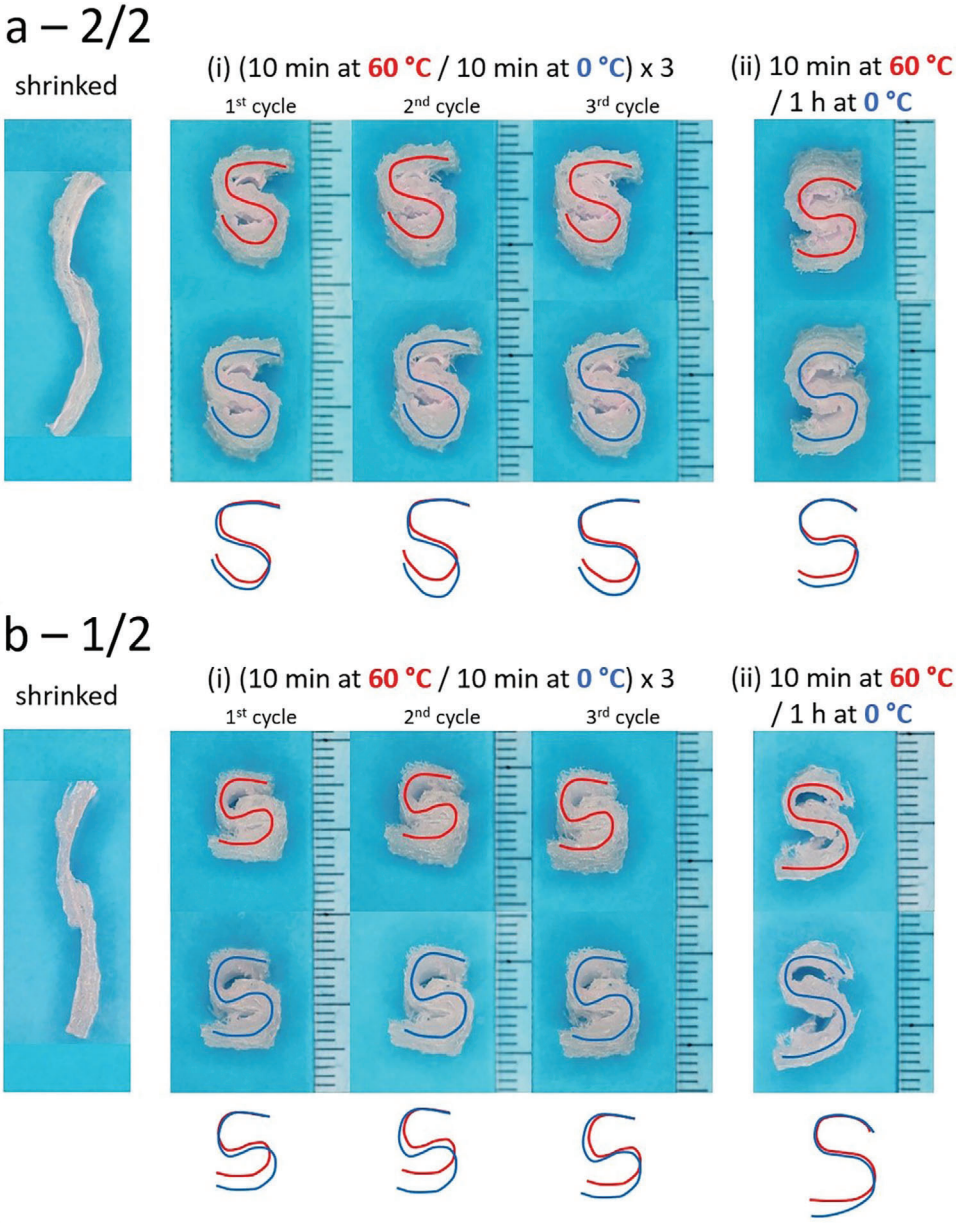

Figure 8. Two-way SME of S-shaped specimens: images of a) 2/2 and b) 1/2 specimens after shrinking at T_{room} and during various thermal cycles.

or heating step following the big transformation at first heating. For each step of the various thermal histories applied, curvature variations are normalized with respect to those occurring at first heating. The resulting average values ($\Delta\kappa_{norm}$) are reported in Figures 7c and 7d, respectively for composites 2/2 and 1/2. Positive values are associated to opening of the C shape (cooling steps) and negative values correspond to its closure (heating steps). The curvature variation during the first cooling phase, which is always smaller compared to the major shape transformation occurring in the first heating phase, is proved to be reversible. In fact, when multiple thermal cycles are applied, the same variation is observed during each following step. Moreover, $\Delta\kappa_{norm}$ varies according to the SMP content and to the cooling temperature and time. For T_{low} = 0 °C, 2/2 composites can recover ≈9–10% of the initial transformation, whereas $\Delta\kappa_{norm}$ of 1/2 specimens is ≈12–15%. The values obtained after cooling for 1 h tend to be slightly higher, but most of the actuation occurs within 10 min at 0 °C. As for samples maintained 1 day at T_{room}, only a very small fraction of the initial transformation is recovered (≈2% and ≈4% for 2/2 and 1/2 specimens, respectively), and even after 1 week, $\Delta\kappa_{norm}$ remains within 4–5%.

A quantitative comparison of these results with respect to other works on the two-way SME of SMP–elastomer composites is not straightforward because the methods employed to evaluate the SME vary from one work to another. For example, Westbrook et al. applied multiple heating–cooling cycles to prestretched SMP strips embedded in an elastomer matrix and fixed at one end, they observed bending of the specimens, and they

calculated that the transversal displacement of the unconstrained end was ≈10% of the specimen length.[16] Chen et al. also photographed the reversible bending movements of their composite actuators, obtained by coupling a stretched shape memory polyurethane layer and an elastic polyurethane layer.[17] Interestingly, Kang et al. created core–shell stretched SMP–elastomer structures that clearly exhibited reversible extension/contraction upon cooling/heating, with actuation strains of ≈10% for core–shell films and ≈20% for core–shell fibers.[18] With respect to all these works, the approach presented in the current paper shows a qualitatively similar response (a first bigger contraction at first heating followed by smaller extension and contraction movements during subsequent cooling and heating steps), but has the distinctive advantage of integrating the pre-stretching of the SMP directly in its production process, thanks to SES on a rotating drum collector.

Other references of interest are works regarding the two-way SME under constant stress for TPU PBA-75 or for other electrospun SMPs. In these cases, higher actuation strains seem to be achieved (up to 40% for TPU PBA-75[23] and up to 70% for electrospun sol–gel crosslinked poly(ϵ-caprolactone)[15]), thanks to the application of a suitable constant stress (in the order of 10^5–10^6 Pa) during heating–cooling cycles. The new 4D fabrication process developed here needs no external stress for reversible actuation upon cooling because the shape transformation at T_{low} is driven by the elastic energy stored in the MEW component. On the other hand, the internal stress at play is more difficult to control; nevertheless, the use of additive manufacturing allows for easy modulation of the MEW structure pattern and thickness, which leaves space for improvement of the reversible actuation strain. Moreover, it should be noted that the cited work on TPU PBA-75[23] adopts a value of T_{low} of −20 °C instead of 0 °C, which may also be helpful in view of increasing the actuation strain.

Finally, S-shaped specimens were investigated as proof-of-concept of the possibility to create 4D objects having more complex geometries with respect to simple bar- and C-shaped specimens found in literature. MEW was performed on both sides of the electrospun mats to introduce multiple curves, with the SMP on the inside and the elastomer on the outside. Once again, 2/2 and 1/2 combinations were selected for the two curves of the S, whereas denser MEW structures (2/2d and 1/2d in Table 1) were deposited on the extremities and in the central part to make them stiffer, and consequently, flatter. Images of the samples after shrinking at T_{room} and during shape memory experiments are shown in **Figure 8**, for two thermal histories: i) 10 min at 60 °C followed by 10 min at 0 °C, repeated for three successive cycles and ii) 10 min at 60 °C followed by 1 h at 0 °C. The longer heating step was necessary because of the high amount of TPU filaments deposited by MEW, forming a dense hydrophobic network that required some time to be penetrated by hot water. All specimens reached the designed S configuration and showed good reversibility of their shape transformation during both types of thermal cycles, confirming the feasibility of modulating the curvature in different areas of the composites and thereby obtaining complex shapes. Such modulation should take into account several parameters, including the total thickness, the SMP/elastomer ratio, the stiffness of both components, and the stretching of the SMP during SES (the pre-stretching can be increased by adopting higher drum rotation speed or larger drum diameter).

3. Conclusion

This paper set the bases of an innovative fabrication method for smart SMP–elastomer composites that evolved in space and time (4D), undergoing bidirectional shape changes in response to thermal stimuli. Electrospinning of the SMP on a drum collector rotating at high speed proved to be an excellent strategy to integrate pre-stretching of the SMP directly in its manufacturing phase, whereas additive manufacturing of the elastomer component by MEW allowed for easy modulation of its structure; in fact, the combination of the elastomer geometric pattern and thickness determined its stiffness, and as a consequence, the final shape of the composite.

Both the SMP/elastomer ratio and the total thickness of the composite were found to play an important role and should be carefully selected to modulate the shapeshifting behavior. When these parameters were properly chosen, a reversible and repeatable SME was achieved. The relatively small actuation amplitude obtained could be ascribed to the tendency of fibrous structures to undergo partially irreversible deformation and dissipate energy (high tan delta value), that was due to bending and displacement of fibers with respect to each other.

There is still space for the SME optimization of these novel systems, which may benefit from experiments on further composite configurations, for example, considering more composition and thickness combinations or also the degree of fiber pre-stretching (depending on the drum collector rotational speed and diameter). Moreover, proof-of-concept experiments on S-shaped specimens open the road toward more complex objects with multiple curvatures, achievable by working on the design of the MEW layers.

In conclusion, this approach appears promising for the development of new flexible and biocompatible smart structures with bidirectional actuation capabilities. These structures may find application as actuators in the field of soft robotics (for example, as clamps/grippers, walkers, crawlers, and so on) or in the biomedical field (for instance, for cell encapsulation, dynamic cell cultures, or smart drug delivery). In the case of soft robotics, the arms or legs of the robots would bend upon heating and unbend upon cooling, allowing grippers to grab and release objects, or walkers and crawlers to progressively move upon multiple actuation cycles. For cell culturing purposes, low triggering temperatures are not expected to significantly reduce cell viability, whereas high triggering temperatures may harm cells, but the increase of the composite curvature can be activated also at ≈40 °C (i.e., close to human body temperature); this would maintain cells alive while extending the time required for shape transformations.

4. Experimental Section

Materials: As SMP, a thermoresponsive polyester urethane was employed. For its synthesis, the following materials were purchased: poly(1,4-butylene adipate) (PBA) diol Desmophen 2505 from Covestro Deutschland AG (Leverkusen, Germany); 4,4′-diphenylmethane diisocyanate (MDI) from Fisher Scientific (Schwerte, Germany); 1,4-butanediol (BD) and a molecular sieve with a pore size of 4 Å from Alfa Aesar (Kandel, Germany). For SES, the following solvents were provided by Merck (Darmstadt, Germany): acetone; dimethylformamide (DMF); chloroform ($CHCl_3$); and tetrahydrofuran (THF). Rhodamine B dye (C.I. 45170) was obtained from Carl Roth GmbH + Co KG (Karlsruhe, Germany).

As elastomer, a commercial thermoplastic polyurethane (TPU) filament was employed. The selected TPU was Filaflex 70A Ultra-Soft by Recreus Industries, S.L. (Elda, Spain).

Synthesis of TPU PBA-75: PBA-based polyester urethane (TPU PBA-75) was synthesized with 75% PBA-based soft segments, following the prepolymer method described in a previous paper.[37] In summary, 0.037 mol of dried PBA-diol and 0.157 mol of MDI reacted at 120 °C for 90 min, forming an isocyanate prepolymer, which then further reacted with 0.12 mol of dried BD. The obtained melt was poured onto a plate covered with a polytetrafluoroethylene film. After a final curing in oven at 80 °C for 120 min, TPU PBA-75 was ground into granules.

Solution Electrospinning (SES) of TPU PBA-75: A custom-made electrospinning device was employed for SES of TPU PBA-75. The setup consisted of a syringe pump (Omnifix 1 mL and 5 mL syringes were used with a 21G needle, that is, having 0.5 mm inner diameter), a 30 kV voltage controller, and a metallic collector (either two conductive bars separated by a 4 cm gap and fixed at 15 cm from the tip of the needle or a rotating drum having a 5 cm diameter and placed at 25 cm from the tip of the needle). Glass slides and aluminum foil were used as substrates for fiber deposition in the case of the two-bar collector and of the rotating drum, respectively.

TPU PBA-75 solutions were obtained by dissolving the polymer granules in different solvent mixtures (DMF-acetone with a volume ratio of 2:3; DMF-$CHCl_3$-THF with volume ratios of 2:2:1), with polymer concentration varying between 6 w/v% and 10 w/v%. A slight amount of rhodamine B was added as dye. The solutions were stirred overnight at ambient temperature and centrifuged for 10 min (8000 rpm, 6010 × *g*, 15 °C), in order to obtain a homogeneous solution.

Looking for the optimal set of process parameters, different values of solution flow rate (0.25–0.5–1 mL h^{-1}) and of applied voltage between the tip of the needle and the collector (20–25–30 kV) were considered. For the rotating drum collector, a speed of 8000 rpm was adopted. For optical microscope observation, the electrospinning process was stopped after ≈5 min, whereas specimens for other analyses had longer production times (30 min to 1 h).

Melt Electrowriting (MEW) of TPU Filaflex: MEW of TPU Filaflex was performed by means of a custom-made device composed of four elements: a three-axis (XYZ) precision stage, a dual-gear feeder system, a thermal control system, and a high voltage supply (LNC 30000, Heinzinger electronic GmbH, Rosenheim, Germany). The control system was created through the software Repetier Host (Hot-World GmbH & Co. KG, Knickelsdorf, Germany). The device was equipped with a 0.2 mm nozzle, which was kept at a 3 mm distance from the collector.

Several parallel long and short filaments were deposited for the selection of optimized process parameters (long filaments: 70 mm length and 1.5 mm spacing; short filaments: 20 mm length and 1 mm spacing; width and height of the filaments were both set to a nominal value of 30 µm in the G-code). The following parameter values were considered: nozzle temperature of 230–240 °C; applied voltage of 1.5–2.5–3.5 kV; collector speed between 300 and 1800 mm min^{-1}.

Composite systems were obtained by deposition of multiple TPU Filaflex layers onto electrospun TPU PBA-75 mats collected on a rotating drum. A quasi-isotropic sequence ($[0°/45°/90°/-45°]_s$) was repeated one or two times. After each set of 4 filament orientations was deposited, the nozzle–collector distance was increased by 0.1 mm. For each orientation, parallel filaments were spaced by 0.5 mm (higher density areas) or 1 mm (standard density areas) and their nominal width and height in the G-code were equal to 30 µm. By changing the thickness or density of the MEW layer in different areas of a same specimen, it was possible to design different shape transformation patterns (see Figure 5). The obtained samples were stored in a freezer at −20 °C.

Optical and Electron Microscopy: Images of fibers obtained by SES and MEW fibers were recorded by means of an optical microscope Eclipse Ti2 (Nikon, Japan) and a scanning electron microscope (SEM) Thermo Fischer Scientific Apreo 2 SEM (USA). Prior to SEM observation, samples were attached onto pin stubs with copper tape, and their conductivity was ensured by sputtering with platinum (≈2 nm) by means of a Leica EM ACE600 (Wetzlar, Germany). Image analyses were carried out by using the software ImageJ (National Institutes of Health, US).

Differential Scanning Calorimetry (DSC): DSC analysis of TPU PBA-75 was carried out with a Mettler Toledo DSC3 (USA). About 10 mg of granules were closed inside an aluminum crucible. The following heating–cooling cycle was repeated four times, each maintaining the sample at a different cooling temperature, T_{low}: i) heating up to 80 °C at 5 °C min^{-1}; ii) maintaining at 80 °C for 5 min; iii) cooling down to T_{low} = (10 °C, 0 °C, −10 °C, or −20 °C) at 5 °C min^{-1}; iv) maintaining at T_{low} for 4 h. A last heating step up to 80 °C at 5 °C min^{-1} completed the analysis.

Preliminary Shrinking Assessments on Electrospun Mats: In order to verify if TPU PBA-75 fibers were sufficiently stretched during the electrospinning process, the shrinking of electrospun mats was observed at room temperature (T_{room}) and at T_{high} = 60 °C. Samples with starting dimensions in the order of 1–2 cm were first detached from the collector at T_{room}, and then, heated up to T_{high}. Pictures of the samples before and after shrinking were taken with a Nikon Coolpix B700 camera, and their dimensions were measured with ImageJ.

Rheological Analyses: The rheological properties of molten TPU Filaflex were evaluated by using the MCR 702 Multidrive Anton Paar (Ostfildern, Germany). Parallel plate geometry of 25 mm diameter was used to measure the viscosity at 230 °C and 240 °C for shear rates between 0.01 and 1000 s^{-1}. A gap of ≈1.5 mm between the plates was adopted.

Shape Memory Experiments: The shape memory behavior of the composites was investigated on two types of samples, designed to take on a C shape (Figure 5a) or an S shape (Figure 5b). C-shaped specimens were obtained by MEW of one or two $[0°/45°/90°/-45°]_s$ sequences with standard density on top of electrospun mats of 1 cm × 1 cm. S-shaped specimens were realized by MEW areas with proper density and thickness on the top and bottom of electrospun mats of ≈3 cm × 1 cm, according to the design reported in Figure 5b.

While the thickness of TPU Filaflex could be easily selected by varying the number of MEW layers, that of TPU PBA-75 varied according to the SES process duration and to the specific position occupied on the surface of the metallic collector. Therefore, for each SES batch, electrospun samples of 2 cm × 2 cm were collected in different positions and weighted. Three mat types were identified as representative of low, medium, or high thickness (nominal weight of 0.5, 1, or 2 mg). MEW samples of 2 cm × 2 cm were also weighted. The mass fraction of SMP (v_{SMP}) could be identified for each thickness combination of TPU PBA-75 and TPU Filaflex, according to the following equation:

$$v_{SMP}\ [\mathrm{wt\%}] = \frac{m_{SMP}}{m_{SMP} + m_E} \times 100 \quad (1)$$

where m_{SMP} is the mass of the SMP (TPU PBA-75) and m_E is the mass of the elastomer (TPU Filaflex).

A Canon EOS 800D camera was used to record the initial shrinking of samples at T_{room}, as well as their reversible shape transformations upon permanence in hot water (T_{high} = 60 °C) or cold water (T_{low} = 0 °C) for selected times. More specifically, a heating step of 3 or 10 min was applied to C-shaped and S-shaped specimens, respectively, and followed by a cooling step of 10 min or 1 h for both sample geometries; in addition, the effect of cooling for 24 h or 1 week in water at T_{room} was explored. In the case of 10 min cooling at T_{low}, three sequential heating–cooling cycles were performed.

For C-shaped samples, a quantitative evaluation of their shape changes was obtained by measuring their curvature (κ) with ImageJ. During the shape memory cycles, the curvature changed from an initial value of 0 m^{-1} to different measured values κ_N, numbered in chronological order (N = 0 after shrinking, N = 1 after the first heating step, N = 2 after the first cooling step, etc.). Normalized curvature variations ($\Delta\kappa_{norm}$) were calculated with respect to the curvature produced by the first heating step, as follows:

$$\Delta\kappa_{norm}\ [\%] = -\frac{\kappa_N - \kappa_{N-1}}{\kappa_1} \times 100 \quad (2)$$

This equation associates positive $\Delta\kappa_{norm}$ values with an opening of the C shape.

Supporting Information

Supporting Information is available from the Wiley Online Library or from the author.

Acknowledgements

This work was supported by Deutsche Forschungsgemeinschaft (DFG) (Grants: IO 68/10-1, IO 68/11-1, IO 68/15-1, IO 68/15-2, IO 68/16-1, IO 68/21-1). T.P. wishes to thank the European Regional Development Fund for financing a large part of the laboratory equipment (project 85007031). Parts of this research were funded by Fraunhofer Cluster of Excellence Programmable Materials (grant numbers PSP elements 40-04068-2500-00007 and 40-03420-2500-00003).

Open access funding enabled and organized by Projekt DEAL.

Conflict of Interest

The authors declare no conflict of interest.

Data Availability Statement

The data that support the findings of this study are available in this article and its Supporting Information or by contacting the author.

Keywords

electrospinning, melt electrowriting, polyester urethane, reversible shape memory effect, shape morphing

Received: January 5, 2024
Revised: March 4, 2024
Published online: March 15, 2024

[1] M. Zare, M. P. Prabhakaran, N. Parvin, S. Ramakrishna, *Chem. Eng. J.* **2019**, *374*, 706.
[2] A. Lendlein, S. Kelch, *Angew. Chem., Int. Ed.* **2022**, *41*, 1973.
[3] A. P. Murcia, J. Manuel, U. Gomez, J.-U. Sommer, L. Ionov, *Macromol. Chem.* **2021**, *54*, 5838.
[4] N. Inverardi N, M. Toselli, G. Scalet, M. Messori, F. Auricchio, S. Pandini, *Macromol. Chem.* **2022**, *55*, 8533.
[5] M. Bothe, T. Pretsch, *J. Mater. Chem.* **2013**, *1*, 14491.
[6] M. Saatchi, M. Behl, U. Nöchel, A. Lendlein, *Macromol. Rapid Commun.* **2015**, *36*, 880.
[7] T. Gong, K. Zhao, W. Wang, H. Chen, L. Wang, S. Zhou, *J. Mater. Chem. B* **2014**, *2*, 6855.
[8] K. A. Davis, K. A. Burke, P. T. Mather, J. H. Henderson, *Biomaterials* **2011**, *32*, 2285.
[9] M. Zare, P. Davoodi, S. Ramakrishna, *Nanomaterials* **2021**, *11*, 933.
[10] L. Wang, F. Zhang, Y. Liu, J. Leng, *Adv. Fiber Mater.* **2022**, *4*, 5.
[11] A. Liguori, S. Pandini, C. Rinoldi, N. Zaccheroni, F. Pierini, M. L. Focarete, C. Gualandi, *Macromol. Rapid Commun.* **2022**, *43*, 2100694.
[12] V. Salaris, A. Leonés, D. Lopez, J. M. Kenny, L. Peponi, *Polymers* **2022**, *14*, 995.
[13] J.-S. Ahn, W.-R. Yu, J. H. Youk, H. Y. Ryu, *Smart Mater. Struct.* **2011**, *20*, 105024.
[14] Q. He, Z. Wang, Y. Wang, Z. Wang, C. Li, R. Annapooranan, J. Zeng, R. Chen, S. Cai, *Sci. Rob.* **2021**, *6*, eabi9704.
[15] S. Pandini, S. Agnelli, A. Merlettini, F. Chiellini, C. Gualandi, K. Paderni, M. L. Focarete, M. Messori, M. Toselli, *Macromol. Mater. Eng.* **2017**, *302*, 1600519.
[16] K. K. Westbrook, P. T. Mather, V. Parakh, M. L. Dunn, Q. Ge, B. M. Lee, H. J. Qi, *Smart Mater. Struct.* **2011**, *20*, 065010.
[17] S. Chen, J. Hu, H. Zhuo, *Compos. Sci. Technol.* **2010**, *70*, 1437.
[18] T.-H. Kang, J.-M. Lee, W.-R. Yu, J. H. Youk, H. W. Ryu, *Smart Mater. Struct.* **2012**, *21*, 035028.
[19] I. Apsite, G. Stoychev, W. Zhang, D. Jehnichen, J. Xie, L. Ionov, *Biomacromolecules* **2017**, *18*, 3178.
[20] D. Chalissery, D. Schönfeld, M. Walter, I. Shklyar, H. Andrae, C. Schwörer, T. Amann, L. Weisheit, T. Pretsch, *Macromol. Mater. Eng.* **2022**, *307*, 2100619.
[21] D. Chalissery, D. Schönfeld, M. Walter, F. Ziervogel, T. Pretsch, *Macromol. Mater. Eng.* **2022**, *307*, 2200214.
[22] G. Constante, I. Apsite, P. Auerbach, S. Aland, D. Schönfeld, T. Pretsch, P. Milkin, L. Ionov, *ACS Appl. Mater. Interfaces* **2022**, *14*, 20208.
[23] M. Bothe, T. Pretsch, *Macromol. Chem. Phys.* **2012**, *213*, 2378.
[24] J. Uribe-Gomez, D. Schönfeld D, A. Posada-Murcia, M. Roland, A. Caspari, A. Synytska, S. Salehi, T. Pretsch, L. Ionov, *Macromol. Biosci.* **2022**, *22*, 2100427.
[25] T. D. Brown, P. D. Dalton, D. W. Hutmacher, *Adv. Mater.* **2011**, *23*, 5651.
[26] T. D. Brown, A. Slotosch, L. Thibaudeau, A. Taubenberger, D. Loessner, C. Vaquette, P. D. Dalton, D. W. Hutmacher, *Biointerphases* **2012**, *7*, 13.
[27] X.-X. He, J. Zheng, G.-F. Yu, M.-H. You, M. Yu, X. Ning, Y.-Z. Long, *J. Phys. Chem.* **2017**, *121*, 8663.
[28] P. D. Dalton, *Curr. Opin. Biomed. Eng.* **2017**, *2*, 49.
[29] H. C. Koch, D. Schmelzeisen, T. Gries, S. Pandini, *Actuators* **2021**, *10*, 31.
[30] S. J. P. Callens, N. Tümer, A. A. Zadpoor, *Appl. Mater. Today* **2019**, *15*, 453.
[31] Z. Ding, C. Yuan, X. Peng, T. Wang, H. J. Qi, M. L. Dunn, *Sci. Adv.* **2017**, *3*, e1602890.
[32] M. Chen, M. Gao, L. Bai, H. Zheng, H. J. Qi, K. Zhou, M. Chen, M. Gao, H. Zheng, K. Zhou, L. Bai, H. J. Qi, *Adv. Mater.* **2023**, *35*, 2209566.
[33] Y. Wang, J. An, H. Lee, *Mol. Syst. Des. Eng.* **2022**, *7*, 1588.
[34] A. Georgopoulou, B. Vanderborght, F. Clemens, *Front. Robot. AI* **2021**, *8*, 615991.
[35] T. Debuissy, E. Pollet, L. Avérous, *Polymer* **2016**, *99*, 204.
[36] G. Hochleitner, A. Youssef, A. Hrynevich, J. N. Haigh, T. Jungst, J. Groll, P. D. Dalton, *BioNanoMaterials* **2016**, *17*, 159.
[37] D. Schönfeld, D. Chalissery, F. Wenz, M. Specht, C. Eberl, T. Pretsch, *Macromol. Chem.* **2021**, *26*, 522.

